Electronic Supplementary Material (ESI) for Journal of Materials Chemistry C.
This journal is © The Royal Society of Chemistry 2015

Supporting information

Tuning the Oxidation Potential of 2-Phenylpyridine-based Iridium Complexes to Improve the Performance of Bluish and White OLEDs

Yafei Wang[†‡Δ], Ning Sun[‖Δ], Basile F. E. Curchod[&], Louise Male[†], Dongge Ma[‖*], Jiang Fan[‡], Yu Liu[‡], Weiguo Zhu[‡*], Etienne Baranoff[†*]

† *School of Chemistry, University of Birmingham, Birmingham B15 2TT, UK*

‡ *Department of Chemistry, Key Lab of Environment-Friendly Chemistry and Application in the Ministry of Education, Xiangtan University, Xiangtan 411105, P. R. China.*

‖ *State Key Laboratory of Polymer Physics and Chemistry, Changchun Institute of Applied Chemistry, Chinese Academy of Sciences, Changchun 130022 , P. R. China*

[&] *Department of Chemistry, Stanford University, Stanford, CA 94305-5080, USA*

[Δ] *The authors contributed equally to this work*

Corresponding authors

DG Ma: mdg1014@ciac.jl.cn

WG Zhu: zhuwg18@126.com

E Baranoff: e.baranoff@bham.ac.uk

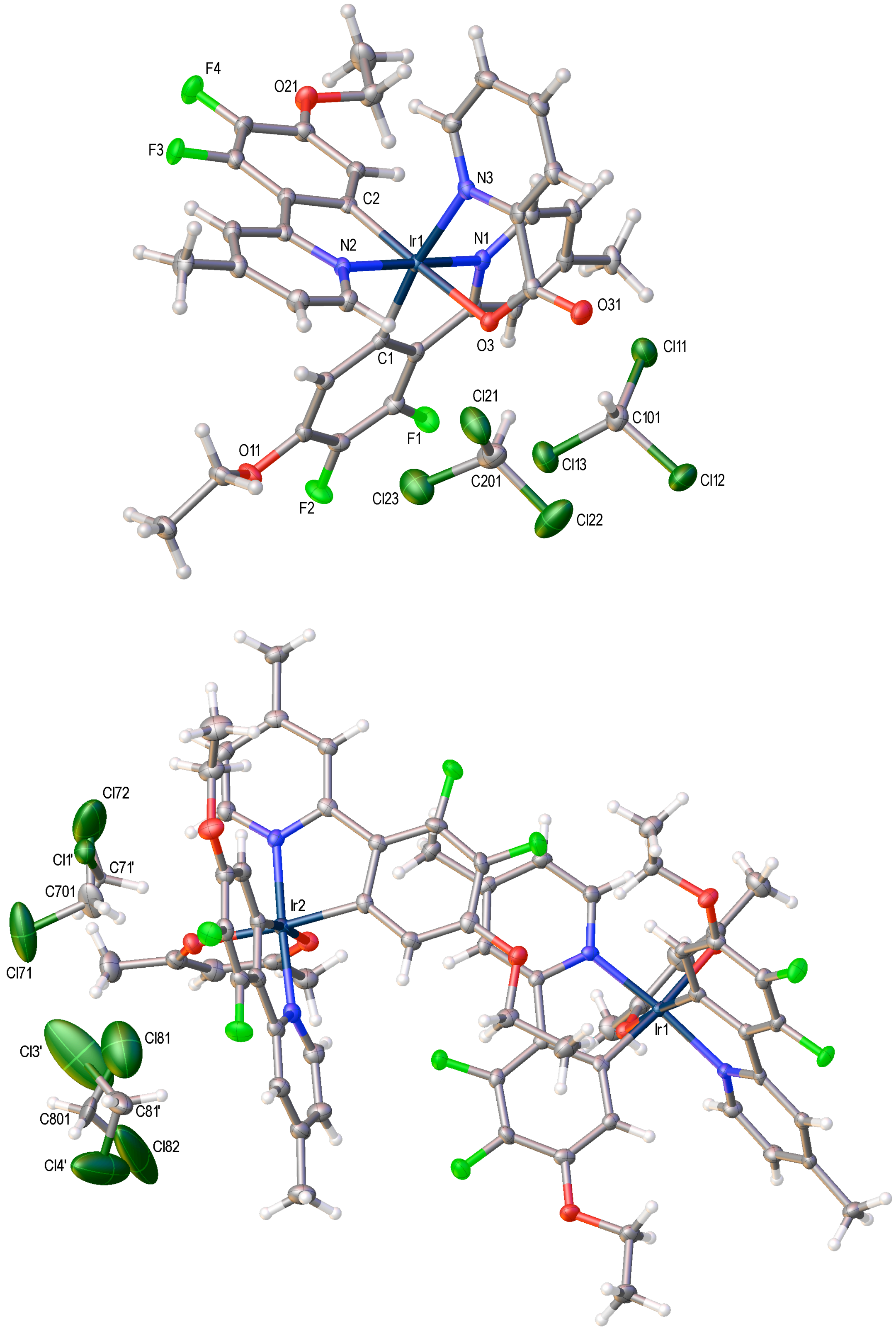

Figure S1. ORTEP representation of the X-ray crystal structures of **YF1** (top) and **YF2** (bottom, showing the two independent molecules of the unit cell).

Table S1. Crystallographic data for **YF1** and **YF2**.

	YF1•2 $CHCl_3$	**YF2•0.5 CH_2Cl_2**
empirical formula	$C_{36}H_{30}Cl_6F_4IrN_3O_4$	$C_{33.5}H_{32}ClF_4IrN_2O_4$
formula weight	1049.53	830.26
temperature, K	100.00(10)	100.00(10)
wavelength (Å)	1.54184	0.71073
crystal system	monoclinic	triclinic
space group	$P2_1/c$	P-1
unit cell dimensions		
a (Å)	11.2797(2)	13.2592(3)
b (Å)	31.1640(5)	17.0439(4)
c (Å)	11.8865(2)	17.1957(4)
α (deg)	90	113.094(2)
β (deg)	111.640(2)	105.6129(19)
γ (deg)	90	99.0525(18)
volume (Å^3)	3883.88(13)	3287.63(14)
Z	4	4
density, calc d (g/cm^3)	1.795	1.677
absorption coefficient (mm^{-1})	11.002	4.205
F(000)	2056.0	1636.0
crystal size (mm^3)	0.1728 × 0.1112 × 0.0814	0.3652 × 0.1003 × 0.0524
2θ range for data collection (deg)	5.672 to 149	6.224 to 52.744
reflections collected	16480	23065
independent reflections	7680 [R_{int} = 0.0279, R_{sigma} = 0.0353]	13313 [R_{int} = 0.0212, R_{sigma} = 0.0389]
data/restraints/parameters	7680/0/491	13313/101/910
goodness-of-fit on F^2	1.012	1.064
final R indices [$I > 2\sigma(I)$]	R_1 = 0.0298	R_1 = 0.0268
	wR_2 = 0.0710	wR_2 = 0.0552
R indices (all data)	R_1 = 0.0339	R_1 = 0.0359
	wR_2 = 0.0738	wR_2 = 0.0601

Computational details

Theoretical calculations. Full geometry optimizations of the iridium compounds in their singlet ground state were performed with density functional theory[2] (DFT) using the PBE0[3] functional with the relativistic effective core potential and basis set LANL2DZ[4] for the iridium, the TZVP[5] basis set for the remaining atoms. Additional calculations for the ground state of both complexes were conducted with the M06[6] functional, using an ultrafine integration. No symmetry constraints were applied during the geometry optimizations, which were carried out with the Gaussian 09 package[7]. The lowest triplet states of the two compounds were optimized using both linear-response time-dependent density functional theory[8] (LR-TDDFT), within the adiabatic approximation[9], and unrestricted DFT (UDFT) calculations, using in all cases the PBE0 functional (additional calculations for the triplet states were also performed with the M05-2X functional[10]) and the aforementioned basis set and effective core potential. Emission energies with LR-TDDFT were obtained using a state-specific approach for solvent effects. Absorption spectra were computed at the ground-state optimized geometry of YF1 and YF2 using LR-TDDFT for the first 40 singlet electronic states and the first 10 triplet states. We note that the exchange and correlation functionals used in this work have been successfully employed in different theoretical studies.[11] The adiabatic ionization energy is obtained by subtracting the energy at the optimized geometry of the cationic complex (UDFT) with the energy of the neutral complex at the optimized ground-state geometry. The nature of the stationary points located with (U)DFT was further checked by analytical computations of harmonic vibrational frequencies at the same level of theory. Condensed-phase effects were taken into account for all calculations (unless otherwise indicated) using a self-consistent reaction-field (SCRF) model in which the solvent is implicitly represented by a dielectric continuum characterized by its relative static dielectric permittivity ε. Within the different approaches that can be followed to calculate the electrostatic potential created by the polarized continuum in the cavity, we have employed the integral equation formalism of the polarizable continuum model (IEFPCM).[12] A relative permittivity of 8.93 was employed to simulate dichloromethane,[7] the solvent used in the experimental work. To facilitate the analysis of LR-TDDFT transitions at the triplet state geometries, we used Natural Transition Orbitals (NTOs)[13], which are obtained through diagonalization of the transition density matrix and constitute the optimal set of orbitals to represent a given electronic transition. The open-source code NANCY_EX-2.0 was used to compute the NTOs[14]. All molecular representations were produced with VMD[15] version 1.9.2.

A note on relativistic effects is required here. While the effective core potential used accounts for scalar relativistic effects, the calculations presented in this work do not include spin-orbit coupling. This approximation is expected to be accurate enough for obtaining a qualitative picture of the electronic structure of these compounds, but will obviously be insufficient to predict quantities such as emission lifetimes and singlet-triplet mixing. It is known, for example, that the MLCT transitions in the absorption spectra are likely to be energetically shifted when spin-orbit coupling is included in the calculations.[11b, 16]

Table S2. Comparison between experimental and theoretical (DFT/M06 and DFT/PBE0) ground state geometries. Selected bond distances (Å) and angles (°)

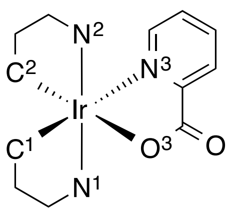				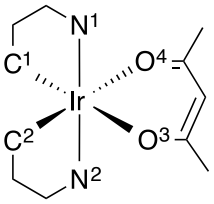			
	X-ray	**M06**	**PBE0**		**X-ray**	**M06**	**PBE0**
Ir-N1	2.038(3)	2.064	2.050	**Ir-N1**	2.031(3)	2.056	2.038
Ir-C1	2.005(3)	2.011	2.007	**Ir-C1**	1.989(3)	1.996	1.991
Ir-N2	2.035(3)	2.054	2.036	**Ir-N2**	2.033(3)	2.056	2.038
Ir-C2	1.990(3)	2.001	1.996	**Ir-C2**	1.975(4)	1.996	1.991
Ir-O3	2.156(2)	2.181	2.156	**Ir-O4**	2.138(2)	2.185	2.159
Ir-N3	2.139(3)	2.183	2.152	**Ir-O3**	2.143(2)	2.185	2.159
N1-Ir-N2	173.77(11)	174.0	175.5	**N1-Ir-N2**	174.96(11)	176.0	177.2

Theoretical characterization

Note: Some of the figures and text are also used in the main text. They are reproduced in this Supporting Information to facilitate the reading of the detailed calculations.

The X-ray structures can be compared with ground-state optimized geometries in gas phase.

The computed Ir-C, Ir-N, and Ir-O bond lengths are in close agreement with the experimental ones (Table S1). More specifically, this level of theory accurately reproduces the slightly longer Ir-C bond length for the ppy ligand *trans* to the picolinate nitrogen. Figure S2 gives a representation of the Kohn-Sham (KS) molecular orbitals computed for the ground-state optimized geometry including implicit solvent effects (see computational details). As expected for cyclometallated iridium complexes[1], the HOMO (highest occupied molecular orbital) of both complexes contains a contribution from the Ir(5d) orbital and extend on the phenyl part of the ppy ligands *via* a π-type orbital, with a small contribution from the fluorine atom in para position with respect to the carbanion. On the other hand, the LUMO (lowest unoccupied molecular orbital) is centered on the ancillary ligand for the **YF1** complex, whereas it is delocalized over both ppy ligands for the **YF2** molecule (a similar orbital corresponds to LUMO+1 and LUMO+2 for **YF1**). Interestingly, the low-lying unoccupied orbitals localized on the ppy ligands display a small contribution from the fluorine atom in meta position, this time, with respect to the carbanion. It is important to note at this stage that the description of these KS molecular orbitals is provided here only to simplify the upcoming analysis of the LR-TDDFT results and should not be taken *per se* as an approximation of the emission character (see below).

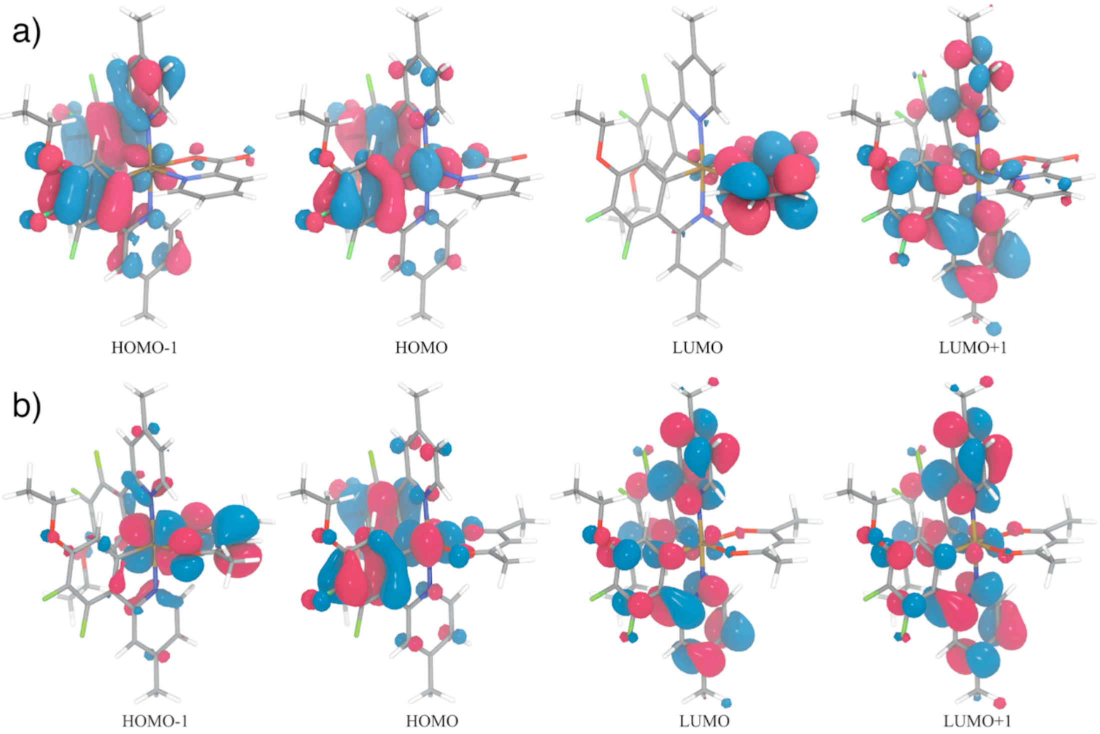

Figure S2. Kohn-Sham molecular orbitals around the HOMO-LUMO gap for the ground-state optimized geometry obtained at the DFT/PBE0/TZVP(LANL2DZ)/IEFPCM(CH_2Cl_2) level of theory. Isovalue set to 0.03. a) **YF1** and b) **YF2**.

The absorption spectra of both complexes were obtained by performing LR-TDDFT calculations at the ground-state optimized geometries. Comparison between experimental absorption spectra in dichloromethane and the computed spectra obtained at the LR-TDDFT/PBE0/TZVP(LANL2DZ)/IEFPCM(CH_2Cl_2) level of theory highlights a rather good correspondence (Figure S3). The first intense transition computed for **YF2** is the one between the ground state (GS) and S_1 (401 nm, $f = 0.0911$), which has a dominant HOMO → LUMO character (95%) and can therefore be qualified as MLCT. Based on the PBE0 functional, the GS → S_1 transition for **YF1** is dark (401 nm, $f = 0.0031$) and displays a HOMO → LUMO character (94%) involving the ancillary ligand (see Figure S2). The first bright transition, according to LR-TDDFT/PBE0, is the GS → S_2 (392 nm, $f = 0.1003$) and has a MLCT character (where L = ppy), as its dominant contribution is HOMO → LUMO+1 (92%). We note that LR-TDDFT/PBE0 reproduces the small shift in energy between the first intense bands of **YF1** and **YF2** observed experimentally. Importantly, some transitions at lower energy are visible from the experimental spectra but are not reproduced theoretically. A possible explanation for this absence could be that those transitions are affected by spin-orbit coupling between singlets and triplets (see Computational Details for a note on this issue), which are neglected in our calculations. Another reason that could potentially lead to this difference is the fact that only the ground-state optimized geometry is used to simulate the absorption spectra. An improvement could be obtained by sampling different nuclear configurations from an approximate Wigner distribution. While this approximation can provide more realistic spectra, it implies a large number of different LR-TDDFT calculations. Work in this direction for a model iridium complex is in progress. LR-TDDFT was then used to compute the low-lying triplet states, still at the ground-state optimized geometry. The first two triplet states of **YF2** are almost degenerate with respect to the ground state (462 nm and 459 nm) and exhibit a MLCT character. Conversely, the transition from the ground state to the first triplet state of **YF1** (at 457 nm) has an important (53%) HOMO → LUMO+1 contribution. This observation implies that the MLCT character of the GS → T_1 transition is mostly related to the ppy ligands and only weakly to the ancillary pic ligand.

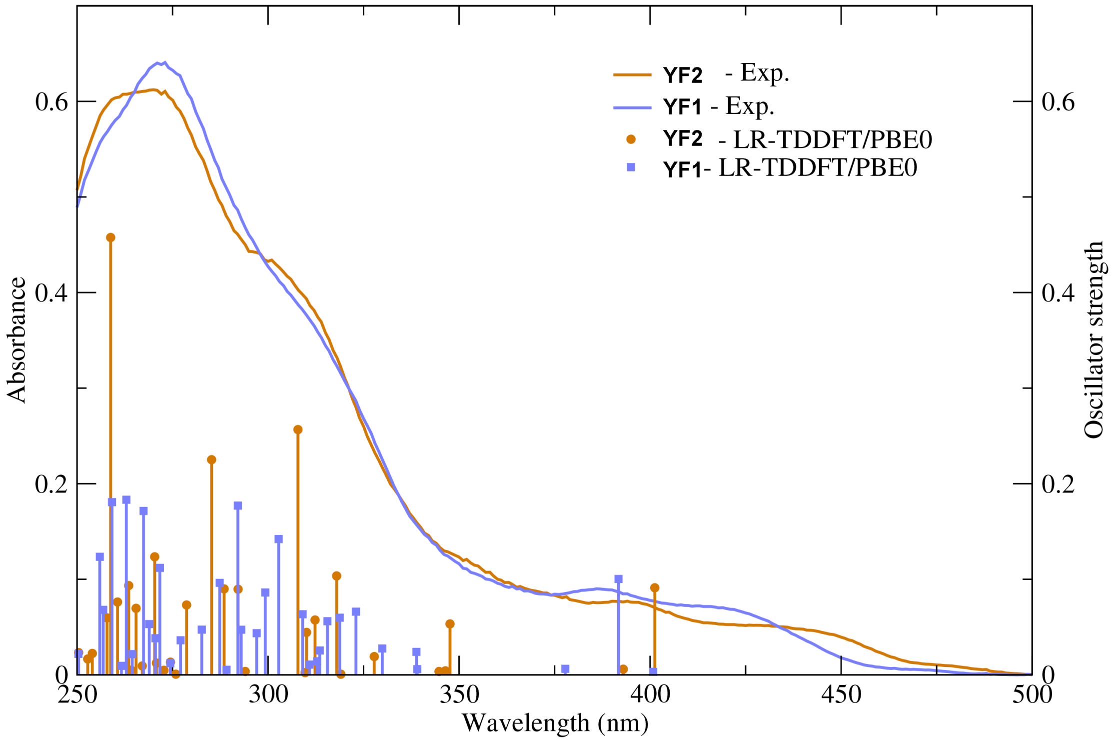

Figure S3. Excitation energies and oscillator strengths computed at the LR-TDDFT/PBE0/TZVP(LANL2DZ)/IEFPCM(CH_2Cl_2) level of theory.

UDFT and LR-TDDFT geometry optimization were performed to shed some lights on the character of the emissive triplet state. Let us first discuss the rather simple case of **YF2**. Geometry optimization of the first triplet state at the LR-TDDFT/PBE0/TZVP(LANL2DZ)/IEFPCM(CH_2Cl_2) level of theory leads to a molecular geometry, at which a triplet-to-singlet transition exhibits a MLCT/LC character. Figure 4a gives the natural transition orbitals (NTOs) characterizing the GS → T_1 transition at this particular triplet geometry and shows that the transition is localized on only one of the ppy ligand. To confirm the LR-TDDFT results, we further optimized the geometry with UDFT/PBE0. The spin density for the T_1 state at this new geometry (Figure 4b) indicates a similar character than what observed with LR-TDDFT.

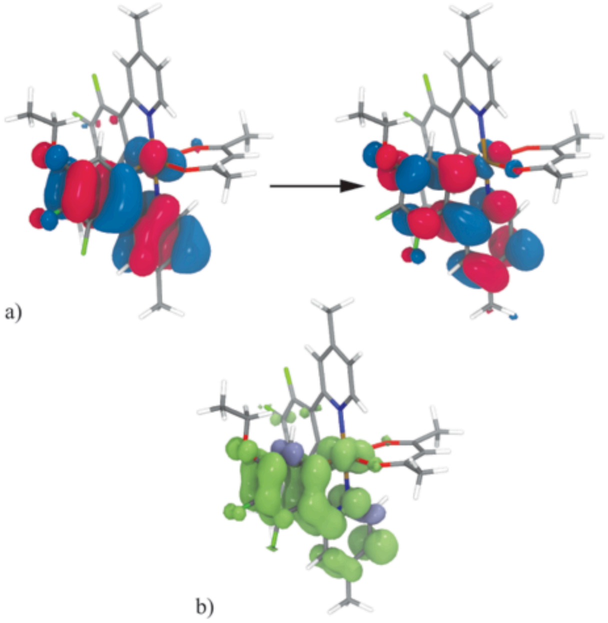

Figure S4. Electronic character at the T1 optimized geometry for **YF2**. a) NTOs representing the GS → T1 at the LR-TDDFT/PBE0/TZVP(LANL2DZ)/IEFPCM(CH_2Cl_2) level of theory. b) contour plot of the spin density at the T1 UDFT/PBE0/TZVP(LANL2DZ)/IEFPCM(CH_2Cl_2) optimized geometry.

We now move on to the **YF1** complex, for which we performed the very same calculations. As for the case of **YF2**, the geometry of the first triplet state obtained with

LR-TDDFT/PBE0/TZVP(LANL2DZ)/IEFPCM(CH_2Cl_2) corresponds to a triplet state with a singlet-to-triplet emission exhibiting a MLCT/LC character (Fig. 4a). The character of this transition is further confirmed by a geometry optimization at the UDFT/PBE0 level, as depicted in Fig. 4b. As for **YF2**, the transition is mostly localized on one ppy ligand. It is however important to note that, contrary to the case of the symmetric **YF2** molecule, the two ppy ligand do not exactly have the same environment in **YF1**, as a result of the asymmetry created by the picolinate ancillary ligand. Therefore, the two triplet states that can be created by populating a different ppy ligand are expected to have a slightly different energy. Optimizing the geometry of the triplet state, whose character implies a transition on the other ppy ligand, leads to a second triplet optimized geometry. The energy difference between the two optimized triplet states, however, lies well within the error of the method (< 2 kJ/mol), as does their respective $T_1 \rightarrow$ GS emission energy. Interestingly, the geometry optimization of the third triplet state leads to a minimum where the MLCT transition involves the pic ligand. This transition is, however, substantially higher in energy than the other two triplet states.

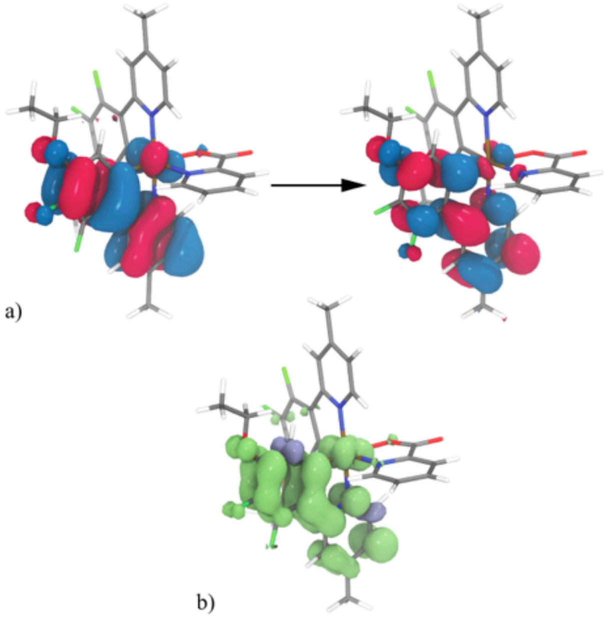

Figure S5. Electronic character at the T_1 optimized geometry for PIC. a) NTOs representing the GS $\rightarrow T_1$ at the LR-TDDFT/PBE0/TZVP(LANL2DZ)/IEFPCM(CH_2Cl_2) level of theory. b) contour plot of the spin density at the T_1 UDFT/PBE0/TZVP(LANL2DZ)/IEFPCM(CH_2Cl_2) optimized geometry.

The experimental maxima of emission are measured at rather similar energies, with 2.56 eV for **YF1** and 2.48 eV for **YF2**. The calculated vertical transitions reproduce this trend between the two compounds, with a value of 2.22 eV (**YF1**) and 2.20 eV (**YF2**) at the LR-TDDFT T1 optimized geometry and 2.37 eV (**YF1**) and 2.35 eV (**YF2**) at the UDFT T_1 minima. (We note that similar calculations using the exchange and correlation functional M05-2X also gave almost degenerate emission energies.) Computing the adiabatic energy difference between the minimum at the T_1 UDFT optimized geometry and the minimum at the GS DFT optimized geometry also gives close values between the two complexes, with an energy of 2.63 eV for **YF1** (2.53 eV including zero-point energy) and 2.59 eV for **YF2** (2.49 eV including zero-point energy), hence reproducing the experimental trends.

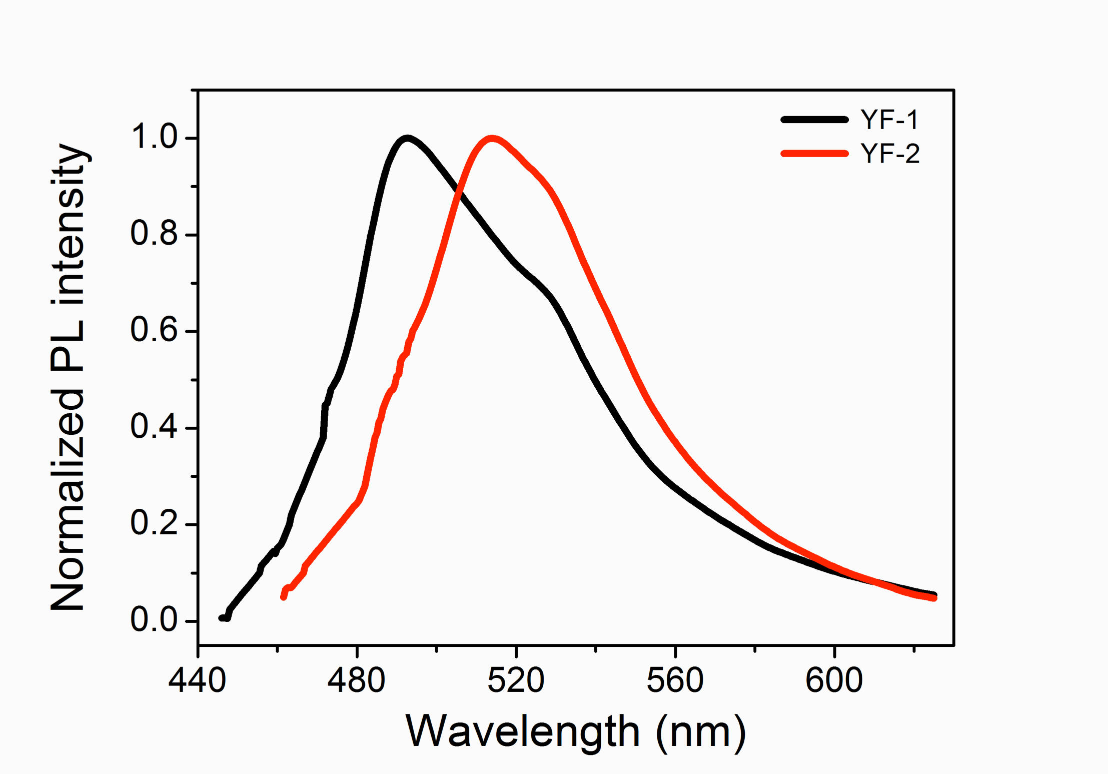

Figure S6. Normalized PL spectra of neat films of the complexes at room temperature.

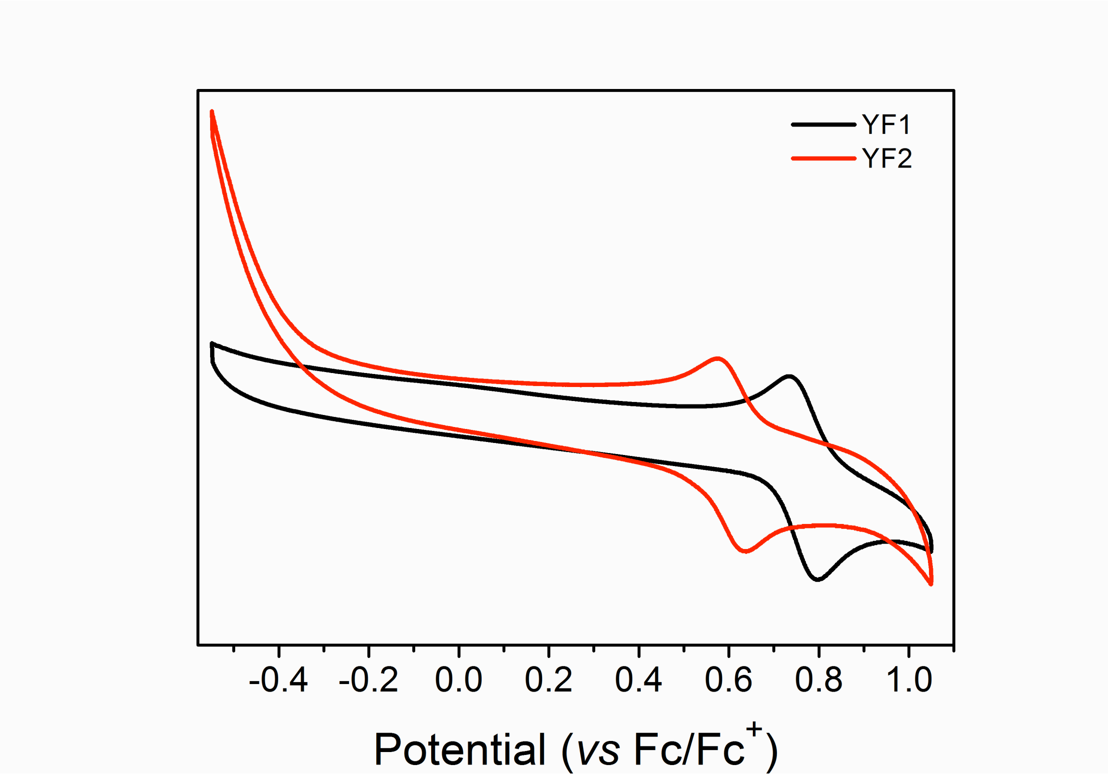

Figure S7. Cyclic voltammograms of iridium complexes in CH_2Cl_2.

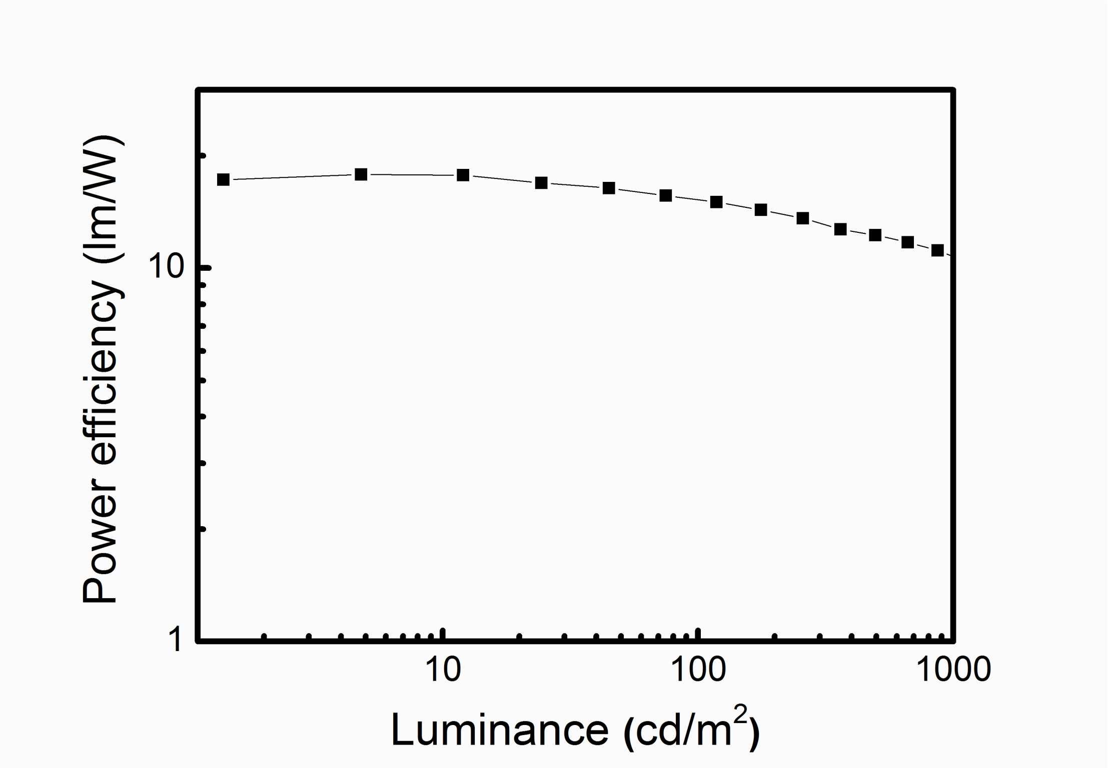

Figure S8. The curve of power efficiency-luminance of **YF1** based device.

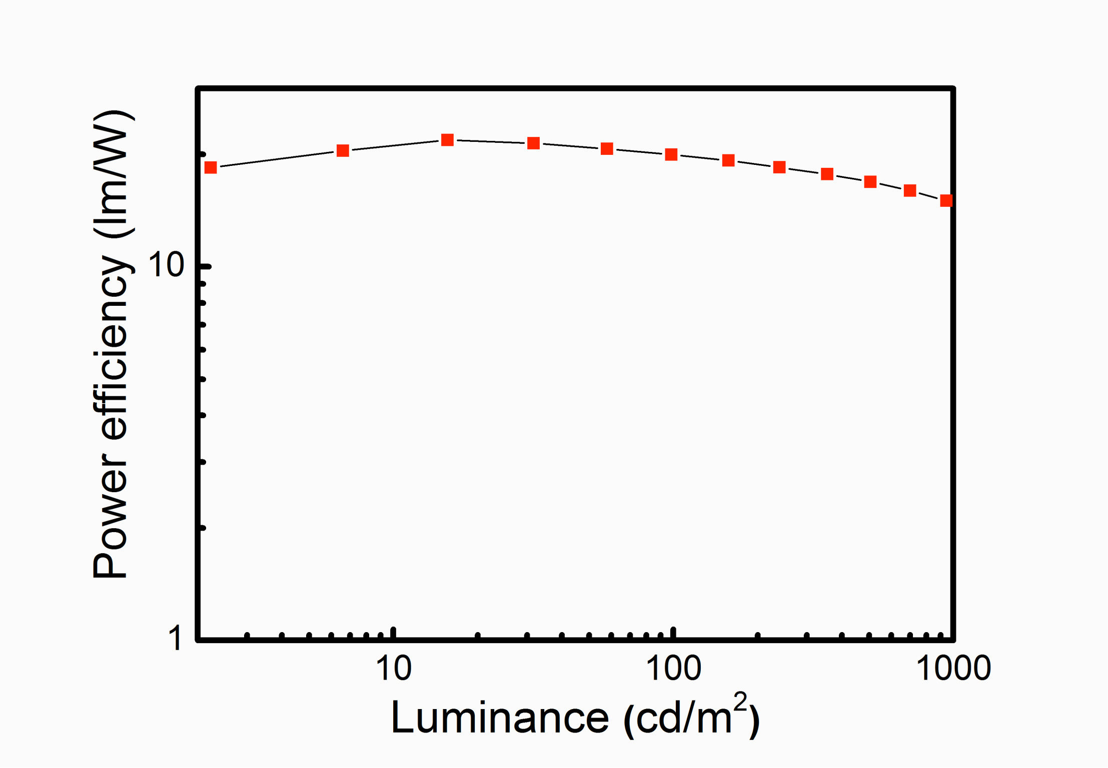

Figure S9. The curve of power efficiency-luminance of **YF2** based device.

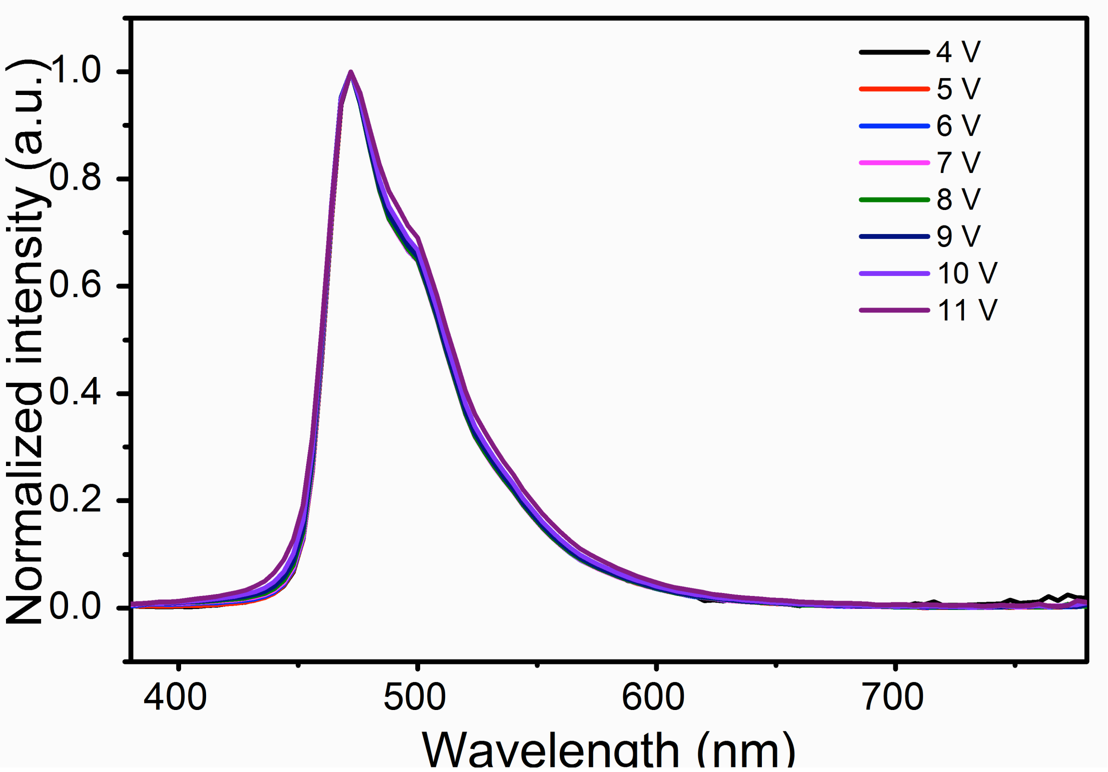

Figure S10. EL spectra of devices for **FIrpic** at different voltages.

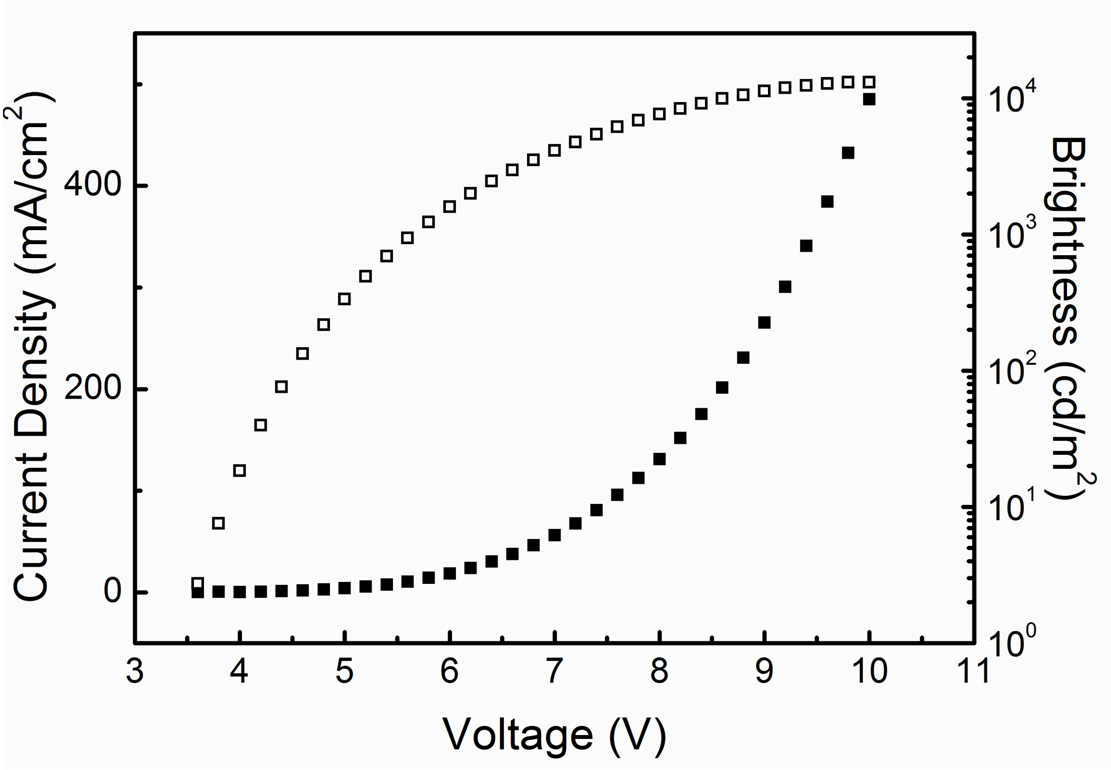

Figure S11. Current density-voltage-brightness (*J*-*V*-*L*) characteristics for **FIrpic**-based device (□: brightness, ■: current density).

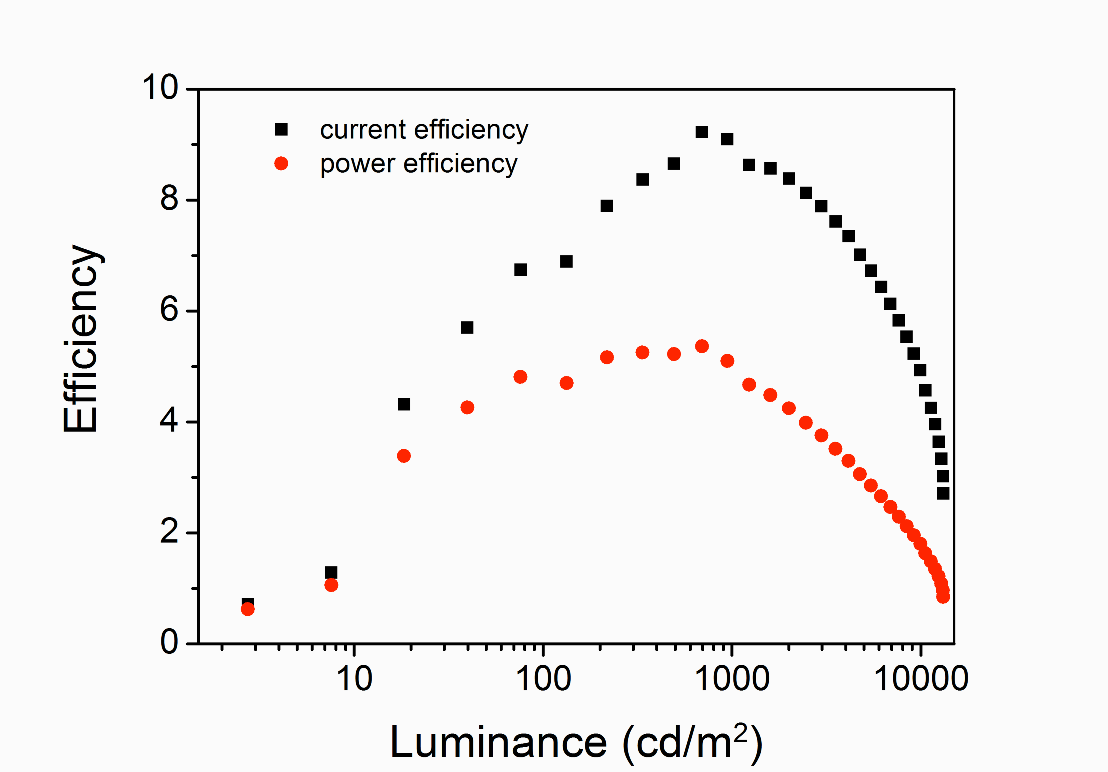

Figure S12. Plots of current efficiency (power efficiency) *vs.* voltage for **FIrpic**-based devices.

Table S3. EL emission and CIE coordinates of devices I-III

Devices	**Applied voltages/V**	λ_{max}**/nm**	**CIE**
I	4	491	(0.1859, 0.5177)
	5	491	(0.1866, 0.5179)
	6	491	(0.1871, 0.5177)
	7	491	(0.1879, 0.5170)
	8	491	(0.1889, 0.5159)
	9	491	(0.1900, 0.5138)
	10	491	(0.1923, 0.5101)
II	4	500	(0.2610, 0.5708)
	5	500	(0.2617, 0.5702)
	6	500	(0.2626, 0.5693)
	7	500	(0.2645, 0.5671)
	8	500	(0.2673, 0.5632)
	9	500	(0.2713, 0.5575)
	10	500	(0.2786, 0.5471)
III	3	56	(0.4320,0.4907)
	4	56	(0.4348,0.4900)
	5	56	(0.4380,0.4896)
	6	56	(0.4403,0.4889)
	7	56	(0.4409,0.4880)
	8	57	(0.4400,0.4870)
	9	58	(0.4374,0.4852)
	10	59	(0.4339,0.4829)

NMR Spectra

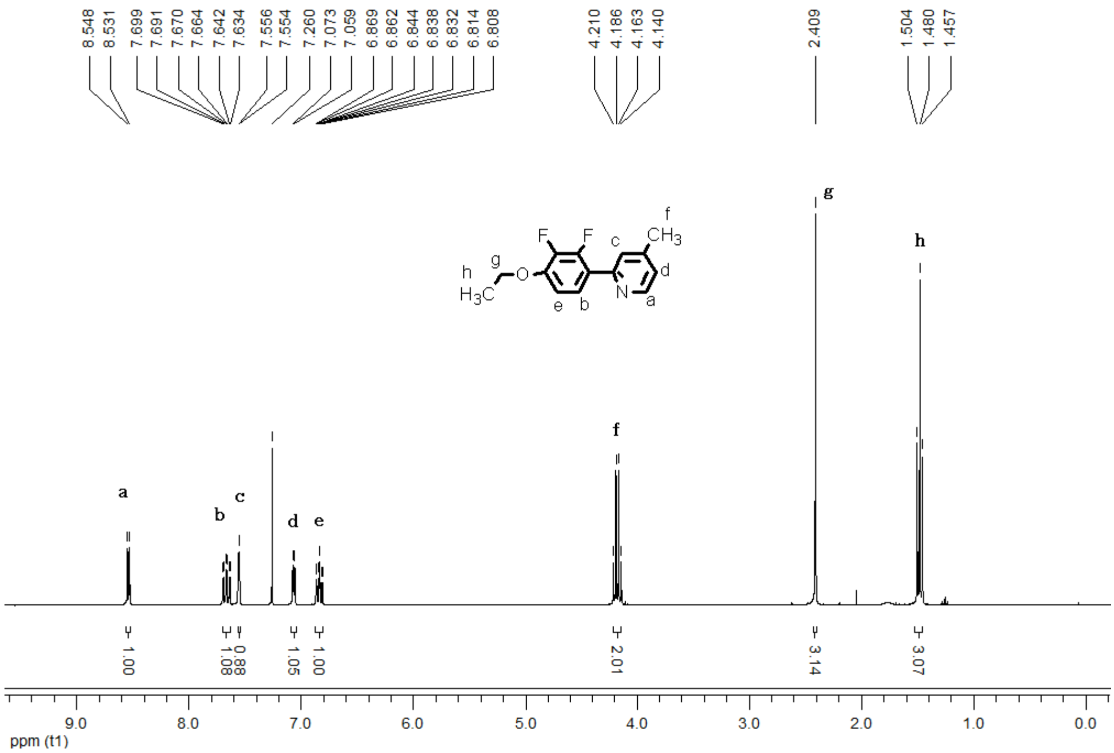
8.548
8.531
7.699
7.691
7.670
7.664
7.642
7.634
7.556
7.554
7.260
7.073
7.059
6.869
6.862
6.844
6.838
6.832
6.814
6.808
4.210
4.186
4.163
4.140
2.409
1.504
1.480
1.457
F
F
c
f
CH3
h
g
O
H3C
d
N
e
b
a
a
b
c
d
e
f
g
h
1.00
1.08
0.88
1.05
1.00
2.01
3.14
3.07
9.0
8.0
7.0
6.0
5.0
4.0
3.0
2.0
1.0
0.0
ppm (t1)

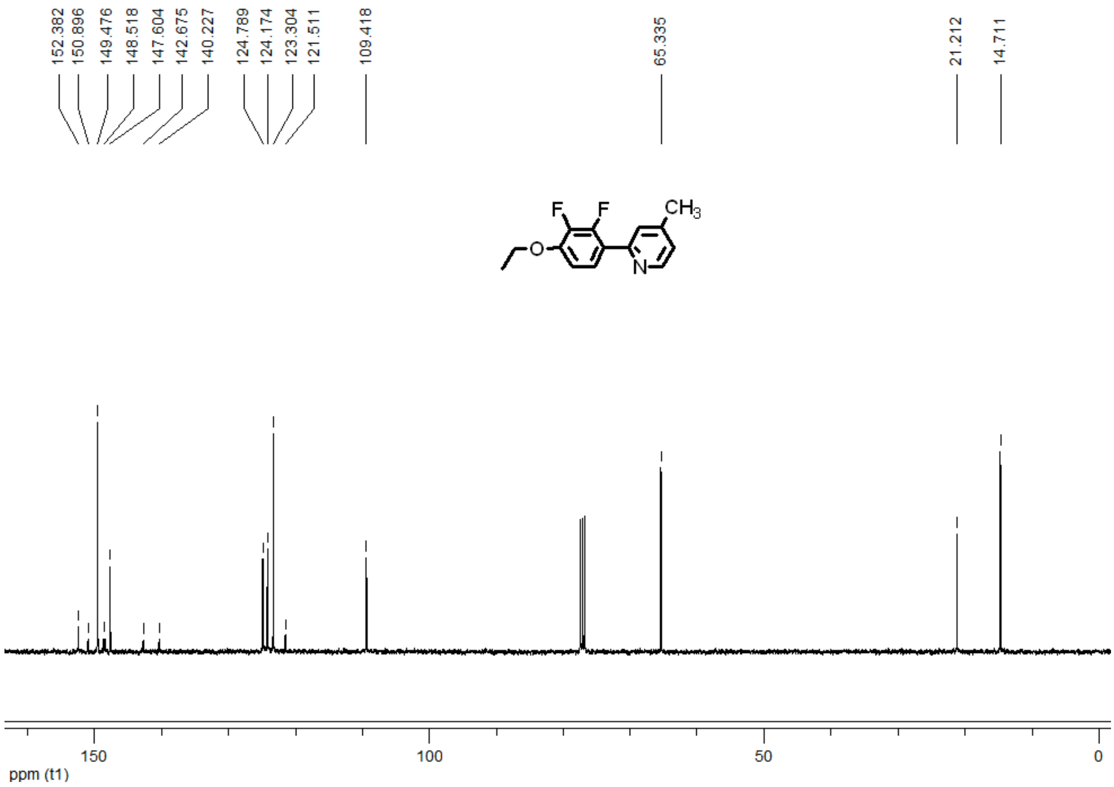
152.382
150.896
149.476
148.518
147.604
142.675
140.227
124.789
124.174
123.304
121.511
109.418
65.335
21.212
14.711
F
F
CH3
O
N
150
100
50
0
ppm (t1)

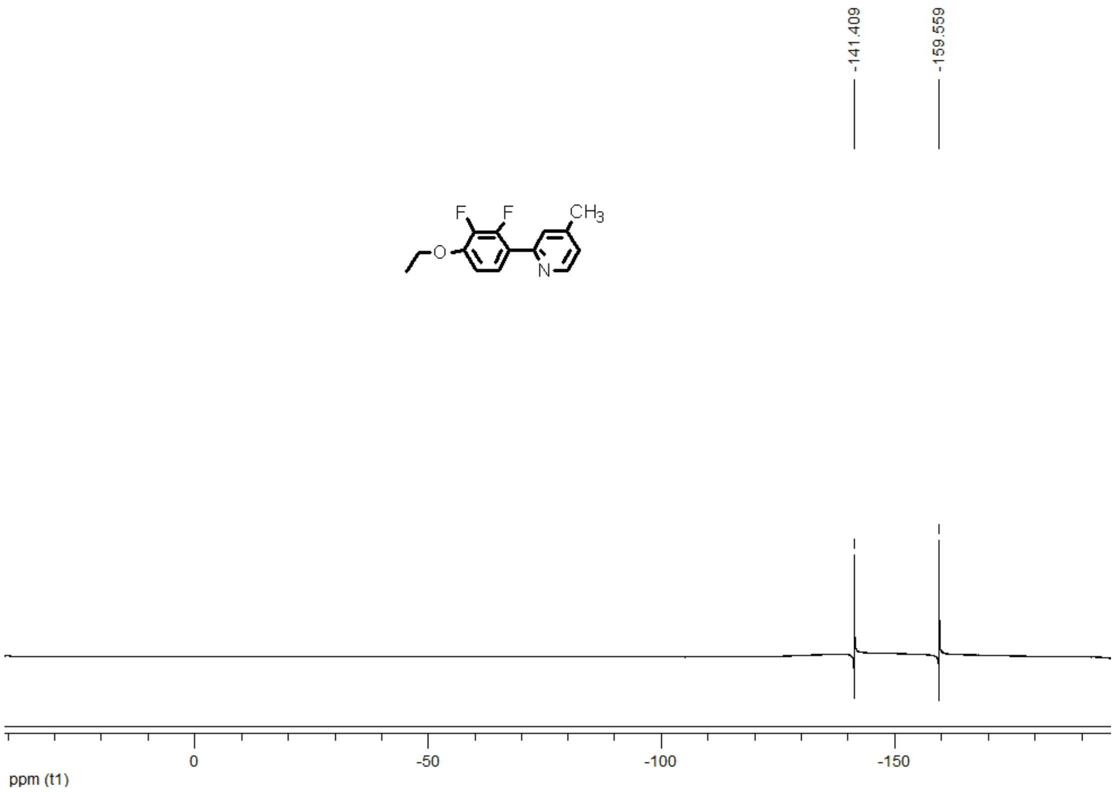
-141.409
-159.559
F
F
CH3
O
N
0
-50
-100
-150
ppm (t1)

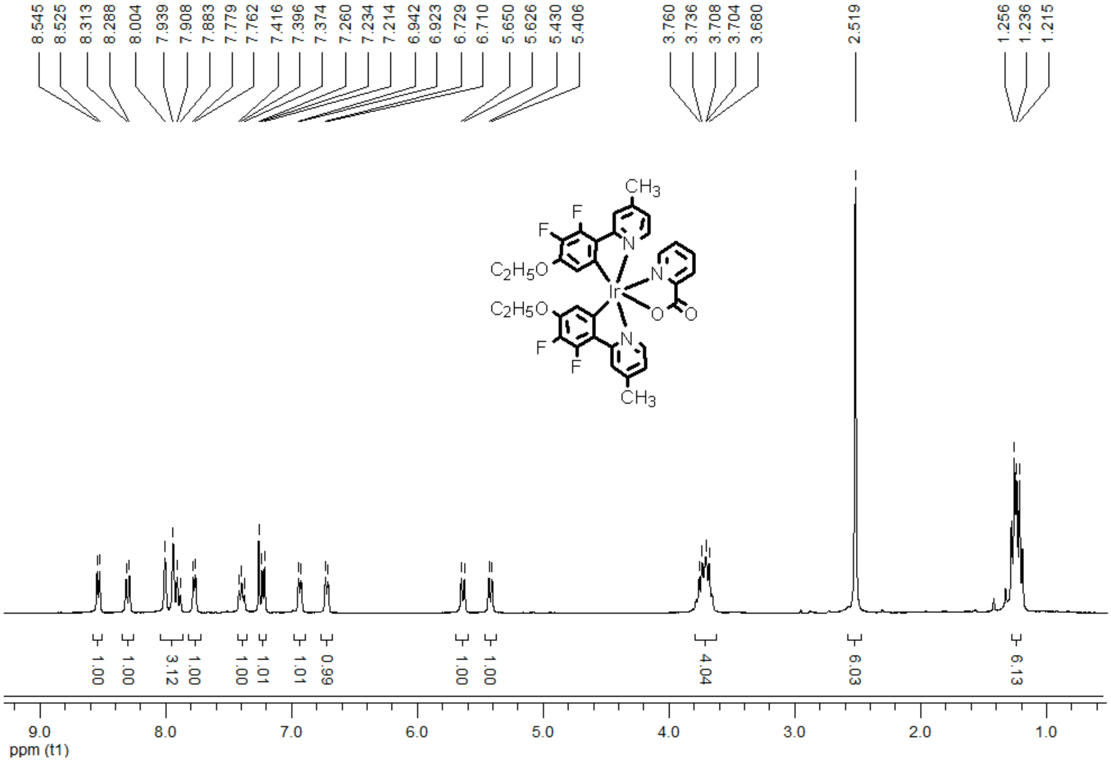
8.545
8.525
8.313
8.288
8.004
7.939
7.908
7.883
7.779
7.762
7.416
7.396
7.374
7.260
7.234
7.214
6.942
6.923
6.729
6.710
5.650
5.626
5.430
5.406
3.760
3.736
3.708
3.704
3.680
2.519
1.256
1.236
1.215
CH3
F
F
N
C2H5O
N
Ir
O
O
C2H5O
N
F
F
CH3
1.00
1.00
3.12
1.00
1.00
1.01
1.01
0.99
1.00
1.00
4.04
6.03
6.13
9.0
8.0
7.0
6.0
5.0
4.0
3.0
2.0
1.0
ppm (t1)

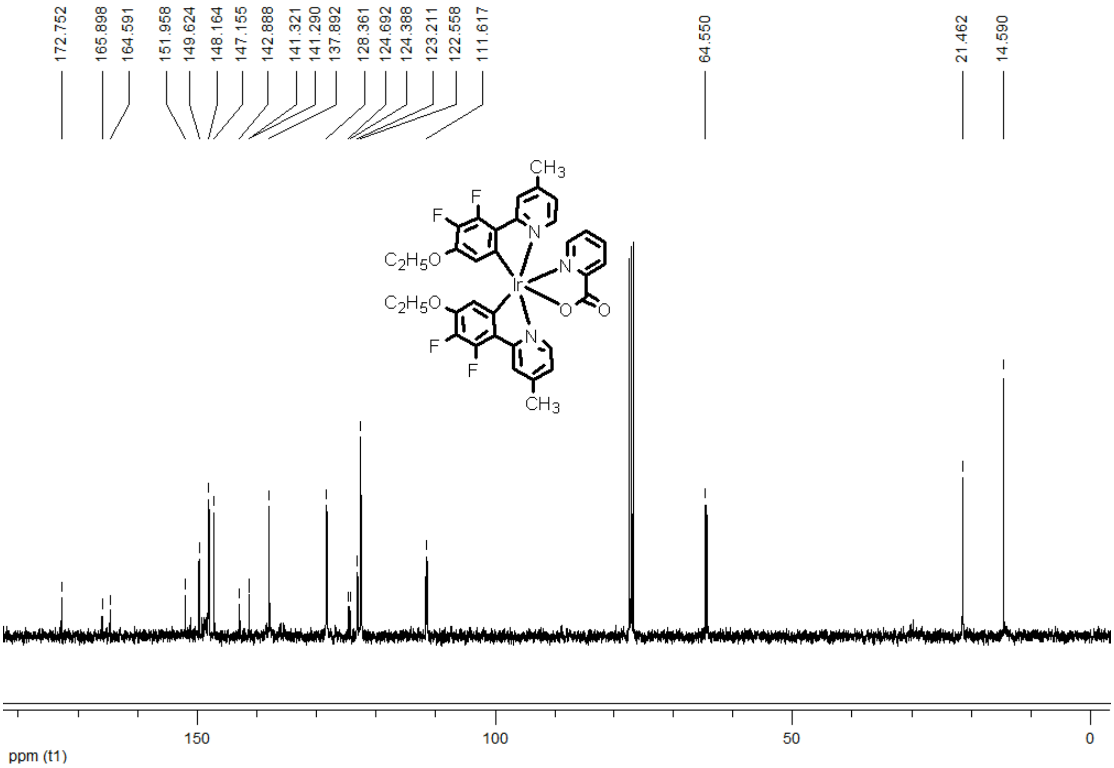
172.752
165.898
164.591
151.958
149.624
148.164
147.155
142.888
141.321
141.290
137.892
128.361
124.692
124.388
123.211
122.558
111.617
64.550
21.462
14.590
CH3
F
F
N
C2H5O
N
Ir
O
O
C2H5O
N
F
F
CH3
150
100
50
0
ppm (t1)

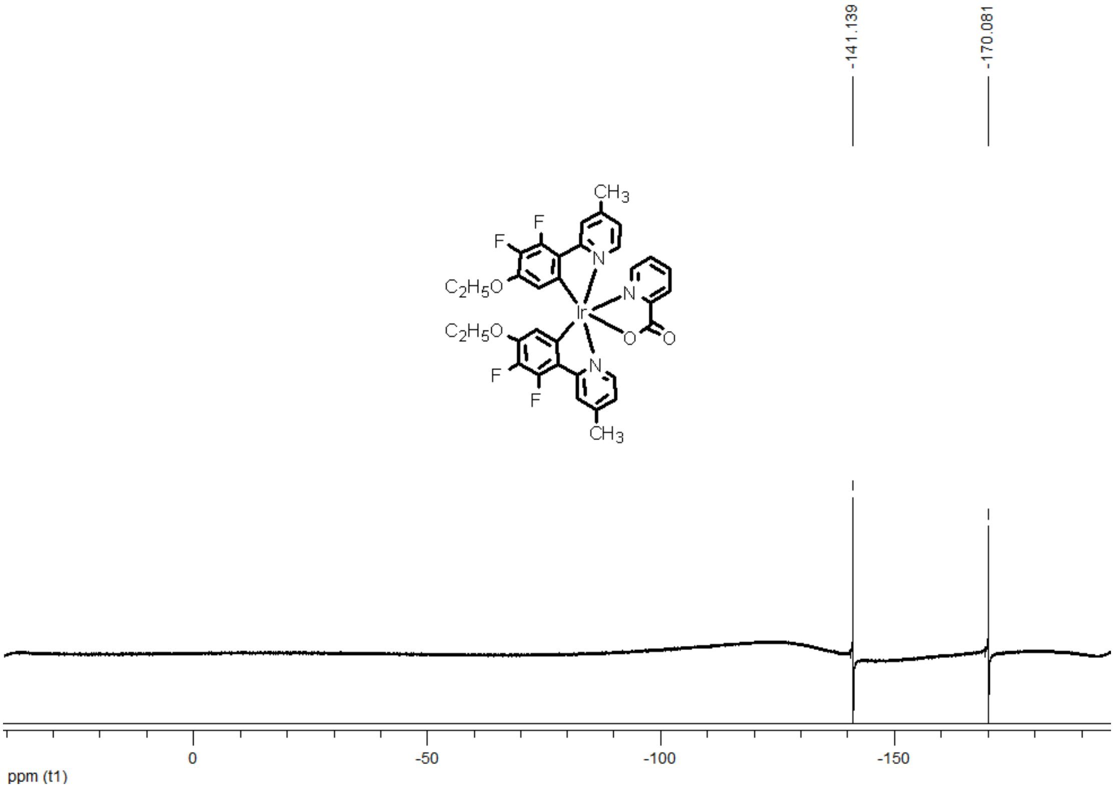
-141.139
-170.081
CH3
F
F
N
C2H5O
N
Ir
O
O
C2H5O
N
F
F
CH3
0
-50
-100
-150
ppm (t1)

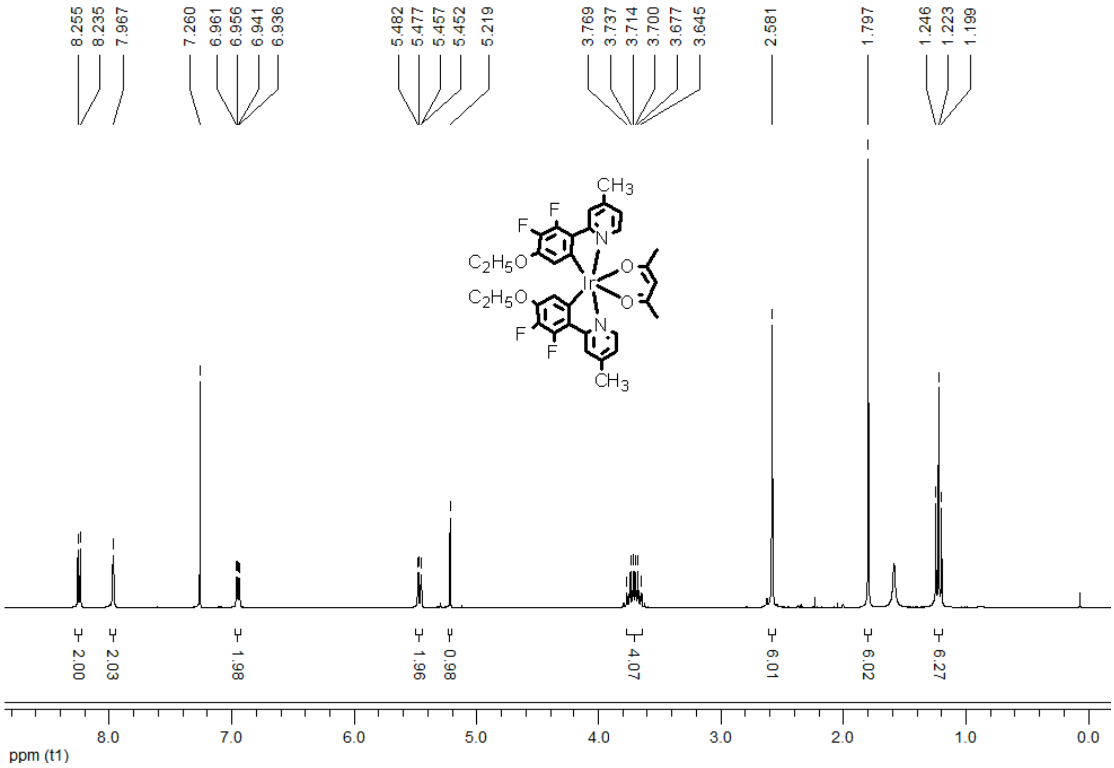
8.255
8.235
7.967
7.260
6.961
6.956
6.941
6.936
5.482
5.477
5.457
5.452
5.219
3.769
3.737
3.714
3.700
3.677
3.645
2.581
1.797
1.246
1.223
1.199
CH3
F
F
N
C2H5O
Ir
O
O
C2H5O
N
F
F
CH3
2.00
2.03
1.98
1.96
0.98
4.07
6.01
6.02
6.27
8.0
7.0
6.0
5.0
4.0
3.0
2.0
1.0
0.0
ppm (t1)

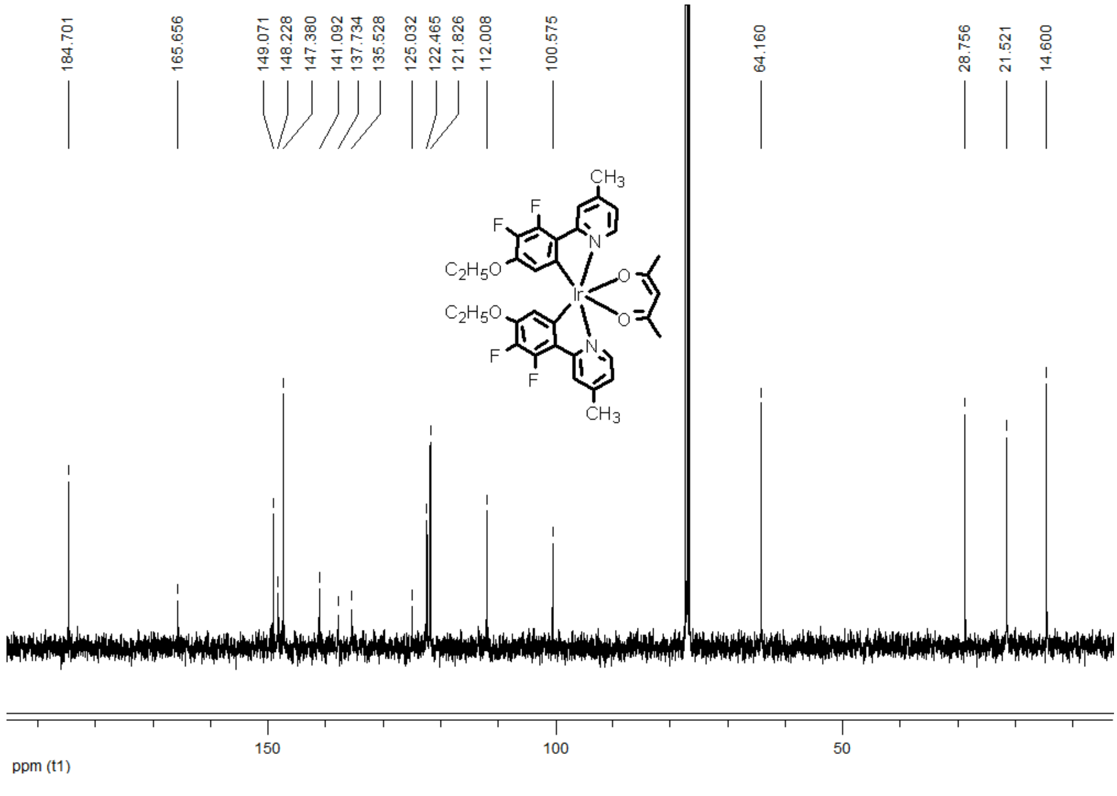
184.701
165.656
149.071
148.228
147.380
141.092
137.734
135.528
125.032
122.465
121.826
112.008
100.575
64.160
28.756
21.521
14.600
CH3
F
F
N
C2H5O
Ir
O
O
C2H5O
N
F
F
CH3
150
100
50
ppm (t1)

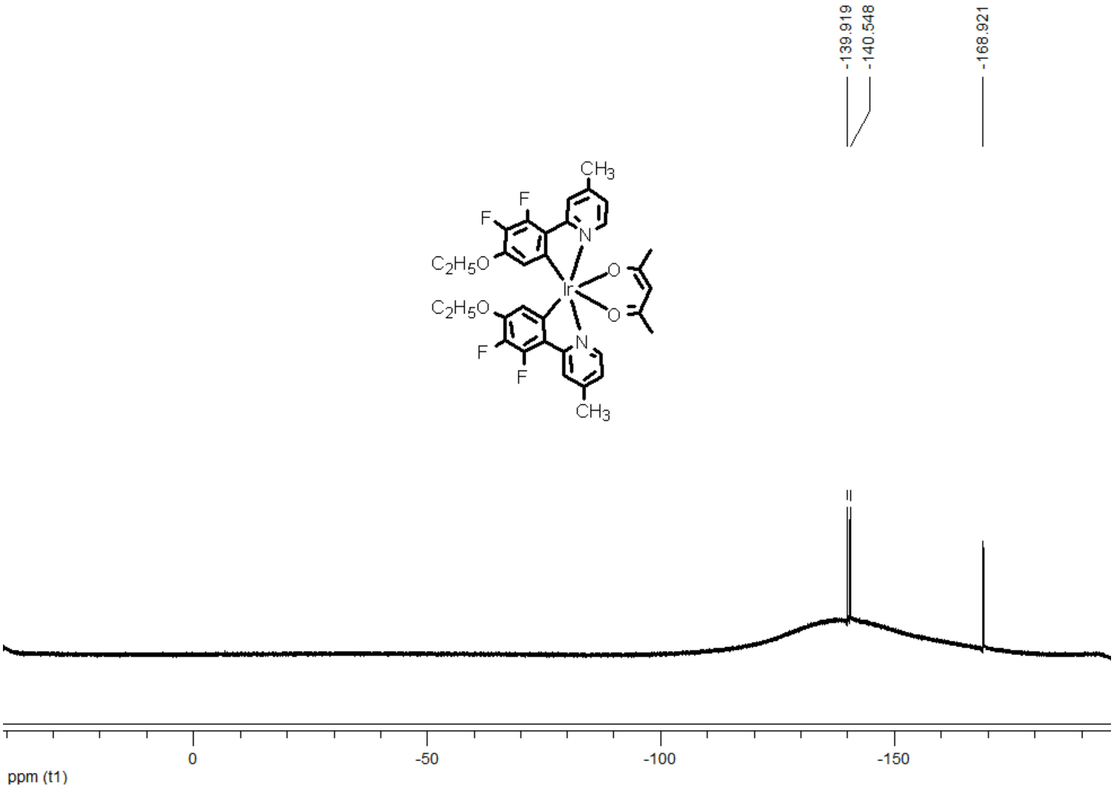
-139.919
-140.548
-168.921
CH3
F
F
N
C2H5O
Ir
O
O
C2H5O
F
F
N
CH3
0
-50
-100
-150
ppm (t1)

References

1. Frey, J.; Curchod, B. F. E.; Scopelliti, R.; Tavernelli, I.; Rothlisberger, U.; Nazeeruddin, M. K.; Baranoff, E., *Dalton Trans.* **2014,** *43*, 5667.

2. (a) Hohenberg, P.; Kohn, W., *Phys. Rev. B* **1964,** *136*, B864; (b) Kohn, W.; Sham, L. J., *Phys. Rev.* **1965,** *140*, 1133.

3. (a) Perdew, J. P.; Burke, K.; Ernzerhof, M., *Phys. Rev. Lett.* **1996,** *77*, 3865; (b) Adamo, C.; Barone, V., *J. Chem. Phys.* **1999,** *110*, 6158.

4. Hay, P. J.; Wadt, W. R., *J. Chem. Phys.* **1985,** *82*, 299.

5. (a) Schaefer, A.; Huber, C.; Ahlrichs, R., *J. Chem. Phys.* **1994,** *100*, 5829; (b) Schafer, A.; Horn, H.; Ahlrichs, R., *J Chem Phys* **1992,** *97* (4), 2571-2577.

6. Zhao, Y.; Truhlar, D. G., *Theor. Chem. Acc.* **2008,** *120*, 215.

7. Frisch, M. J.; Trucks, G. W.; Schlegel, H. B.; Scuseria, G. E.; Robb, M. A.; Cheeseman, J. R.; Scalmani, G.; Barone, V.; Mennucci, B.; Petersson, G. A.; Nakatsuji, H.; Caricato, M.; Li, X.; Hratchian, H. P.; Izmaylov, A. F.; Bloino, J.; Zheng, G.; Sonnenberg, J. L.; Hada, M.; Ehara, M.; Toyota, K.; Fukuda, R.; Hasegawa, J.; Ishida, M.; Nakajima, T.; Honda, Y.; Kitao, O.; Nakai, H.; Vreven, T.; Montgomery, J., J. A.; Peralta, J. E.; Ogliaro, F.; Bearpark, M.; Heyd, J. J.; Brothers, E.; Kudin, K. N.; Staroverov, V. N.; Kobayashi, R.; Normand, J.; Raghavachari, K.; Rendell, A.; Burant, J. C.; Iyengar, S. S.; Tomasi, J.; Cossi, M.; Rega, N.; Millam, J. M.; Klene, M.; Knox, J. E.; Cross, J. B.; Bakken, V.; Adamo, C.; Jaramillo, J.; Gomperts, R.; Stratmann, R. E.; Yazyev, O.; Austin, A. J.; Cammi, R.; Pomelli, C.; Ochterski, J. W.; Martin, R. L.; Morokuma, K.; Zakrzewski, V. G.; Voth, G. A.; Salvador, P.; Dannenberg, J. J.; Dapprich, S.; Daniels, A. D.; Farkas, A.; Foresman, J. B.; Ortiz, J. V.; Cioslowski, J.; Fox, D. J., Gaussian09 Revision D.

8. (a) Casida, M. E., Time-dependent density-functional response theory for molecules. In *Recent Advances in Density Functional Methods*, Chong, D. P., Ed. Singapore, World Scientific: 1995; p 155; (b) Runge, E.; Gross, E. K. U., *Phys. Rev. Lett.* **1984,** *52*, 997; (c) Petersilka, M.; Gossmann, U. J.; Gross, E. K. U., *Phys. Rev. Lett.* **1996,** *76*, 1212.

9. Ullrich, C. A., *Time-Dependent Density-Functional Theory*. Oxford University Press: 2012.

10. Zhao, Y.; Schultz, N. E.; Truhlar, D. G., *J Chem Theory Comput* **2006,** *2*, 364.

11. (a) Baranoff, E.; Curchod, B. F. E.; Frey, J.; Scopelliti, R.; Kessler, F.; Tavernelli, I.; Rothlisberger, U.; Gratzel, M.; Nazeeruddin, M. K., *Inorg. Chem.* **2012,** *51*, 215; (b) Baranoff, E.; Curchod, B. F. E.; Monti, F.; Steimer, F.; Accorsi, G.; Tavernelli, I.; Rothlisberger, U.; Scopelliti, R.; Grätzel, M.; Nazeeruddin, M. K., *Inorg. Chem.* **2012,** *51*, 799; (c) Li, H. F.; Winget, P.; Risko, C.; Sears, J. S.; Bredas, J. L., *Phys. Chem. Chem. Phys.* **2013,** *15*, 6293; (d) Swiderek, K.; Paneth, P., *J. Phys. Org. Chem.* **2009,** *22*, 845.

12. Tomasi, J.; Mennucci, B.; Cammi, R., *Chem. Rev.* **2005,** *105*, 2999.

13. Martin, R. L., *J. Chem. Phys.* **2003,** *118*, 4775.

14. Etienne, T.; Assfeld, X.; Monari, A., *J. Chem. Theory Comput.* **2014,** *10*, 3896.

15. Humphrey, W.; Dalke, A.; Schulten, K., *J. Mol. Graph.* **1996,** *14*, 33.

16. Kleinschmidt, M.; van Wullen, C.; Marian, C. M., *J. Chem. Phys.* **2015,** *142*, 094301.